Standard in vitro evaluations of engineered bone substitutes are not sufficient to predict in vivo preclinical model outcomes

Author(s):
Hatt, Luan P.; Armiento, Angela R.; Mys, Karen; Thompson, Keith; Hildebrand, Maria; Nehrbass, Dirk; Müller, Werner E.G.; Zeiter, Stephan; Eglin, David; Stoddart, Martin J.

Publication date:
2023-01-15

Permanent link:
https://doi.org/10.3929/ethz-b-000594932

Originally published in:
Acta Biomaterialia 156, https://doi.org/10.1016/j.actbio.2022.08.021

Acta Biomaterialia 156 (2023) 177–189

Contents lists available at ScienceDirect

Acta Biomaterialia

journal homepage: www.elsevier.com/locate/actbio

Full length article

Standard *in vitro* evaluations of engineered bone substitutes are not sufficient to predict *in vivo* preclinical model outcomes☆

Luan P. Hatt[a,b,1], Angela R. Armiento[a,1,2], Karen Mys[a], Keith Thompson[a,2], Maria Hildebrand[a], Dirk Nehrbass[a], Werner E.G. Müller[c], Stephan Zeiter[a], David Eglin[d], Martin J. Stoddart[a,*]

[a] AO Research Institute Davos, 7270 Davos Platz, Switzerland
[b] Institute for Biomechanics, ETH Zürich; 8093 Zürich, Switzerland
[c] Institute for Physiological Chemistry, University Medical Center of the Johannes Gutenberg University, Mainz, Germany
[d] Mines Saint-Etienne, Univ Lyon, Univ Jean Monnet, INSERM, U 1059 Sainbiose, Centre CIS, F-42023 Saint-Etienne, France

ARTICLE INFO

Article history:
Received 1 April 2022
Revised 10 August 2022
Accepted 11 August 2022
Available online 19 August 2022

Keywords:
Biomaterials
Bone
Preclinical models
Translational science
Osteogenesis

ABSTRACT

Understanding the optimal conditions required for bone healing can have a substantial impact to target the problem of non–unions and large bone defects. The combination of bioactive factors, regenerative progenitor cells and biomaterials to form a tissue engineered (TE) complex is a promising solution but translation to the clinic has been slow. We hypothesized the typical material testing algorithm used is insufficient and leads to materials being mischaracterized as promising. In the first part of this study, human bone marrow – derived mesenchymal stromal cells (hBM-MSCs) were embedded in three commonly used biomaterials (hyaluronic acid methacrylate, gelatin methacrylate and fibrin) and combined with relevant bioactive osteogenesis factors (dexamethasone microparticles and polyphosphate nanoparticles) to form a TE construct that underwent *in vitro* osteogenic differentiation for 28 days. Gene expression of relevant transcription factors and osteogenic markers, and von Kossa staining were performed. In the second and third part of this study, the same combination of TE constructs were implanted subcutaneously (cell containing) in T cell-deficient athymic Crl:NIH-*Foxn1*^{rnu} rats for 8 weeks or cell free in an immunocompetent New Zealand white rabbit calvarial model for 6 weeks, respectively. Osteogenic performance was investigated via MicroCT imaging and histology staining. The *in vitro* study showed enhanced upregulation of relevant genes and significant mineral deposition within the three biomaterials, generally considered as a positive result. Subcutaneous implantation indicates none to minor ectopic bone formation. No enhanced calvarial bone healing was detected in implanted biomaterials compared to the empty defect. The reasons for the poor correlation of *in vitro* and *in vivo* outcomes are unclear and needs further investigation. This study highlights the discrepancy between *in vitro* and *in vivo* outcomes, demonstrating that *in vitro* data should be interpreted with extreme caution. *In vitro* models with higher complexity are necessary to increase value for translational studies.

Statement of significance

Preclinical testing of newly developed biomaterials is a crucial element of the development cycle. Despite this, there is still significant discrepancy between *in vitro* and *in vivo* test results. Within this study we investigate multiple combinations of materials and osteogenic stimulants and demonstrate a poor correlation between the *in vitro* and *in vivo* data. We propose rationale for why this may be the case and suggest a modified testing algorithm.

☆ Part of the Special Issue on Biofabrication for Orthopedic, Maxillofacial, and Dental Applications, guest-edited by Professors Hala Zreiqat, Khoon Lim, and Debby Gawlitta.

* Corresponding author at: AO Research Institute Davos, Clavadelerstrasse 8, 7270 Davos Platz, Switzerland.
E-mail address: martin.stoddar@aofoundation.org (M.J. Stoddart).

[1] These authors contributed equally to the work.

[2] Current address for Angela R. Armiento and Keith Thompson: UCB Pharma, SL1 3WE Slough, UK.

https://doi.org/10.1016/j.actbio.2022.08.021

1. Introduction

Considering its complex structure, bone is a tissue with a surprising regenerative capacity. Growth factors, multiple cell types and mechanical forces synergistically contribute to the healing process. While it is evident that bone can heal, it is still not clear why this is not always the case. Non-healing fractured bones (non-unions) and large bone defects of various pathological nature have serious healthcare implications across the population and represent challenging medical conditions for orthopaedic surgeons.

This clinical scenario has triggered a quest to identify the optimal conditions required for bone healing. The result is a multitude of tissue engineering (TE) approaches, combining various cell types and functional biomaterials in the presence of bioactive molecules, to create *in vitro* models of bone healing and to develop new therapies to restore lost bone [1]. Among the numerous natural biomaterials investigated, fibrin is easily obtained by the reaction of fibrinogen and thrombin, while hyaluronic acid (HA) and gelatin are widely used in their methacrylated form (MeHA and GelMA, respectively), which allows light-mediated tunable crosslinking. Cells are also frequently encapsulated in these materials, particularly bone marrow-derived mesenchymal stromal cells (BM-MSCs). BM-MSCs have emerged as the archetypal cell in bone TE due to their relative ease of isolation and capacity *in vitro* to differentiate into relevant cell types for bone repair, such as chondrocytes and osteoblasts.

In vitro protocols for osteogenic differentiation of human BM-MSCs were originally established in the late 1990s [2] and continue to represent one of the fundamental assays to demonstrate MSC multilineage potential. The osteogenic cocktail contains β-glycerophosphate (BGP), dexamethasone (Dexa) and ascorbic acid, supplemented to serum-containing culture medium. Within the osteogenic cocktail, ascorbic acid is essential for collagen fibrillation, while BGP provides an organic source of phosphate for hydroxyapatite deposition during mineralization. Inorganic alternatives to BGP are continuously investigated to obtain an optimum calcium:phosphate ratio more akin to that of carbonated hydroxyapatite present in human bone [3] and to have stable levels of free P_i levels during the *in vitro* culture [4]. Among the inorganic P_i sources, polyphosphates (polyP) are an effective substitute to BGP for osteogenic differentiation of human BM-MSCs in monolayer [5] and has been shown to be effective during bone formation *in vivo* [6]. During *in vitro* osteogenic differentiation, Dexa is essential for mineralization, although, the specific contribution of Dexa to stimulate human BM-MSC osteogenesis *in vitro* at the molecular level remains to be adequately described. Both 10 and 100 nM doses of Dexa are currently used [7] with the lower dose considered more physiologically relevant, while the magnitude of cellular response varies across donors [8].

Despite numerous attempts at developing new biomaterials for bone regeneration, there have been few successes achieving clinical translation. A European multicentre analysis has reported a lack of correlation between *in vitro* and *in vivo* outcome with a surprisingly high failure of translation for biomaterials in the orthopaedic field [9]. Part of the reason for this may be the approaches commonly used to investigate the potential of new materials to repair bone. Strict guidelines are lacking and the International Organization of Standardization (ISO) protocols for Biological Evaluation of Medical Devices only requires *in vitro* cytotoxicity tests according to ISO 10993-1:2018 (Biological evaluation of medical devices — Part 1: Evaluation and testing within a risk management process).

In this study we follow a widely used approach to test biomaterials for TE purposes and demonstrate specific examples of promising *in vitro* TE constructs that fail to translate to the *in vivo* setting. We have employed one cell type (human BM-MSCs), three different biomaterials based on natural components of bone fracture callus (HA and fibrin) and extracellular matrix (collagen), and two bioactive molecules (Dexa and polyP). We start with an *in vitro* osteogenic differentiation assay and then proceeded to test these biomaterials in typically used *in vivo* model systems: a cell containing ectopic subcutaneous implantation in nude rats, and a cell free orthotopic calvarial defect model in rabbits.

The results clearly show that standard *in vitro* evaluations are not sufficient to predict or justify follow up animal models and more representative *in vitro* tests are warranted to reduce the number of unproductive and expensive preclinical studies.

2. Material and methods

Unless otherwise stated all reagents are from Sigma-Aldrich.

2.1. Ethical approval

Human MSCs used for both the *in vitro* experiment and the subcutaneous model are isolated from the bone marrow aspirate of a female patient (age 28) upon written consent and approval of Freiburg ethical committee (418/19).

All animal procedures are approved by the ethical committee of Grisons (Switzerland) and performed according to the Swiss Animal Protection Law in an AAALAC International-accredited facility (Authorization Number: GR2018_11 and 17_2019).

2.2. Fabrication of PCL microspheres loaded with Dexa

Poly(ε-caprolactone) (PCL) microspheres loaded with Dexa are fabricated following a previously described method with minor modifications [10]. A total of 400 mg PCL (MW: 80,000 g/mol) is dissolved in 15 mL dichloromethane (DCM; Carl Roth) and 100 mg dexamethasone (Dexa, TCI Chemicals) is dissolved in 8 mL acetone. After 1 hour under moderate stirring, the two solutions are mixed. To create an emulsion, 1% poly(vinyl alcohol) (PVA; MW: 30000 g/mol) is used as aqueous phase. The PCL/Dexa solution is added dropwise to 100 mL of PVA solution, and the emulsion is obtained by probe sonication (Bandelin Sonopuls GM70) on ice with three bursts of 10 seconds at 700 W. The organic phase is allowed to evaporate overnight at room temperature under moderate stirring. To remove any agglomerate, the resulting microspheres are filtered using a 70 µm cell strainer and the dispersion is centrifuged for 15 min at 37700 x g using an ultracentrifuge (Optima XE-90, Beckman Coulter). The collected microspheres are washed in Milli-Q® water to remove the excess of the PVA surfactant and thoroughly dispersed by sonication and re-collected by ultracentrifugation. After two washes, the microspheres are dispersed in Milli-Q® water, lyophilized, sterilized using ethylene oxide gas and stored at -20°C until use. SEM image of Dexa-laden PCL microparticles is presented in Supplementary Figure 1.The yield is quantified as dry weight of the microspheres.

To quantify the amount of encapsulated Dexa, high performance liquid chromatography (HPLC) is performed. The lyophilized microspheres are dissolved in a cosolvent system of 80/20 methanol/DCM to a concentration of 1 mg/mL. The DCM solvent is allowed to evaporate overnight at room temperature and the next day the volume is adjusted with methanol to reach the previous concentration of 1 mg/mL. The PCL is precipitated and removed via filtration and the Dexa remained solubilized in methanol. A standard curve is prepared using a solution of Dexa in methanol: 100, 30, 20, 15, 10, 5 and 2 µg/mL. All solutions are filtered with 0.22 µm Phenex syringe filters (Phenomenex) before loading in the HPLC (Agilent Technologies 1260 Infinity). UV absorption is measured at 239 nm. The efficiency of encapsulation is calculated according to the following equation: $EE\% = (Dexa_{encapsulated}/Dexa_{initial}) \times 100\%$. $Dexa_{encapsulated}$ is the

Table 1
MSCs-laden biomaterials with and without particles.

Group	Dexa-loaded microspheres (mg/mL)	PolyP nanoparticles (µg/mL)
1	-	-
2	10	-
3	-	30
4	10	30

dexa: dexamethasone, polyp: polyphosphate.

amount of Dexa quantified via HPLC and $Dexa_{initial}$ is the amount of Dexa added to the emulsion. Three independent batches are fabricated following the described procedure.

2.3. In vitro *release of Dexa from PCL microspheres*

A total of 10 mg of Dexa-loaded microspheres is incubated in 1 mL of phosphate buffered saline (PBS) at 37°C under mild shaking. At each time point (0.5, 1, 2, 4, 6, 8, 24, 48, 96 h and 5, 6, 7, 8, 11, 12, 13, 15 and 20 days), the samples are centrifuged at 12000 x g for 10 min and the supernatant is removed and replaced with 1 mL fresh PBS. The Dexa released is quantified via HPLC using a standard curve as described in the previous section (2.2).

2.4. *Synthesis of methacrylate hyaluronic acid and gelatin*

Methacrylated hyaluronic acid (MeHA) is synthesized according to previously reported protocol [11]. Briefly, hyaluronic acid sodium salt from *Streptococcus equi* (280 kDa, Contipro Biotech S.R.O.) is fully dissolved at 5% (w/v) in distilled water at room temperature. Methacrylic anhydride (MA) is added dropwise to the hyaluronic acid solution under vigorous stirring. The solution is allowed to react for 4 h under stirring and the pH is maintained between 7.5 and 8.5. After overnight stirring the solution is dialyzed against distilled water for 1 week. The solution is lyophilized and stored at -20°C until use.

Gelatin methacryloyl (GelMA) is synthesized through the reaction of gelatin and MA, as described previously [12]. Briefly, type A porcine skin gelatin (Bloom 180) is mixed at 10% (w/v) into PBS at 60°C and stirred until fully dissolved. MA is added dropwise to the gelatin solution (0.14 mL/g of gelatin) under stirring conditions at 50°C. The solution is allowed to react for 3 h at 50°C and then is diluted 5 times with PBS. The mixture is dialyzed against distilled water using 12-14 kDa cut-off dialysis tubing for 1 week at 40°C to remove unreacted MA. The solution is lyophilized and stored at -20°C until use.

The degree of methacrylation of MeHA and of GelMA is quantified by 1H nuclear magnetic resonance (NMR) as 47% and 55%, respectively. NMR spectra are presented in Supplementary Figure 2. Before cell encapsulation and animal surgeries, the lyophilized materials are sterilized using ethylene oxide gas.

2.5. In vitro *osteogenic differentiation within 3D hydrogels*

2.5.1. *Cell encapsulation and osteogenic differentiation*

Human bone marrow derived MSCs are isolated and cryopreserved according to established protocol [13]. Upon thawing, the cells are expanded until passage 3 as previously described [5]. MeHA (2% w/v) and GelMA (8% w/v) are dissolved in Irgacure (0.3% w/v) solution. Fibrinogen (28 mg/mL) is prepared in 0.9% NaCl containing 1000 U aprotinin (Carl Roth). All the solutions are kept at 37°C until cell encapsulation. For each biomaterial four groups are created (Table 1): 1. Biomaterial + cells (MSCs); 2. Biomaterial + cells + 10 mg/mL Dexa-loaded microspheres (MSCs + Dexa); 3. Biomaterial + cells + 30 µg/mL polyP nanoparticles (MSCs + polyP); and 4. Biomaterial + cells + 10 mg/mL Dexa-loaded microspheres + 30 µg/mL polyP (MSCs + Dexa + polyP). MSCs are suspended in MeHA, GelMA or fibrinogen (± Dexa and/or polyP) at a final density of 20×10^6 cells/mL. Cylindrical cell-laden hydrogels (100 µL volume; containing 2×10^6 cells) are produced in 4% (w/v) agarose moulds, created using a 6 mm diameter biopsy punch (Braun). MeHA and GelMA are subsequently crosslinked within a BioLink® BLX 365 irradiation system (Witec AG) at 1 J, for 1.5 min and 10 min, respectively. The cell-laden fibrinogen is then supplemented with thrombin (1:1 volume) just before casting into the moulds and clotting is obtained at 37°C within 30 min. The final concentration of fibrinogen, aprotinin and thrombin is 14 mg/mL, 500 U/mL and 2 U/mL, respectively.

Cell-laden hydrogels are pre-incubated in osteocontrol (OC) medium (Dulbecco's Modified Eagle Medium (DMEM 1 g/L glucose, Gibco), 10% FBS (Gibco), and 100 U/mL plus 100 µg/mL penicillin and streptomycin, respectively) for the first 24 h. After this period (day 0), the samples are cultured in OC medium supplemented with the osteogenic cocktail (10 nM dexamethasone, 50 µg/mL ascorbic acid 2-phosphate and 10 mM β-glycerophosphate). 6-Aminocaproic acid (5 µM) is added to the culture medium of fibrin gels to reduce the cell-induced shrinkage. Medium change is performed three times per week and cultures are repeated with 3 technical replicates for each group and analysis.

2.5.2. *RNA isolation and RT-qPCR*

Cell-laden hydrogels are harvested at day 0 and 28 and RNA is extracted according to previously described protocol [14] with modifications for fibrin gels. Briefly, MeHA and GelMA samples are pulverized, lysed in TRI-Reagent® (1 mL/sample, supplemented with 5 µL/mL of Polyacryl Carrier; both Molecular Research Center Inc.) and homogenized using QIAShredder columns (Qiagen). Fibrin samples are directly lysed in TRI-Reagent® and homogenized using QIAShredder columns. Phase separation and precipitation is obtained using 1-bromo-3-chloropropane (BCP) and isopropanol, respectively. Gene expression analysis is carried out using two-step reverse transcription quantitative polymerase chain reaction (RT-qPCR). Total RNA (250 ng) is reverse transcribed using random hexamers and SuperScript™ VILO™ (Invitrogen), according to manufacturer's instructions and real time qPCR is carried out using TaqMan® Universal Master Mix with 5 ng of cDNA in a 10 µL reaction volume. Each PCR reaction is performed in technical triplicates for 40 cycles using a QuantStudio® 6 Flex Real-Time PCR System (Applied Biosystems®). Primers used are listed in Supplementary Table 1. Data are analyzed according the $\Delta\Delta$Ct method using *RPLP0* as normalizer and day 0 samples as calibrator.

2.5.3. *Cytological preparation and von Kossa staining*

At day 0 and day 28 cell-laden hydrogels are rinsed in PBS and fixed in 10% neutral buffered formalin for 24 h. Samples are rinsed in tap water and transferred to 5% sucrose solution in PBS at 4°C. After overnight incubation, the samples are embedded in cryocompound and sectioned (12 µm) using a Microm HM560 cryostat (Thermo Fisher Scientific® Inc.). Von Kossa staining is carried out according to the routine protocol. Briefly, the sections are brought to deionized water and then flooded with 5% silver nitrate aqueous solution for 30 min while exposed to strong natural light. After a wash in deionised water, the sections are treated with 5% sodium thiosulfate for 10 min and then washed again with running tap water first and deionized water after. Nuclear fast red is used as a counterstain. The sections are then dehydrated in an ethanol gradient, cleared in xylene and mounted using Eukitt® Quick-hardening mounting medium. Images are acquired using BX63F light microscope equipped with a DP74 digital camera (Olympus).

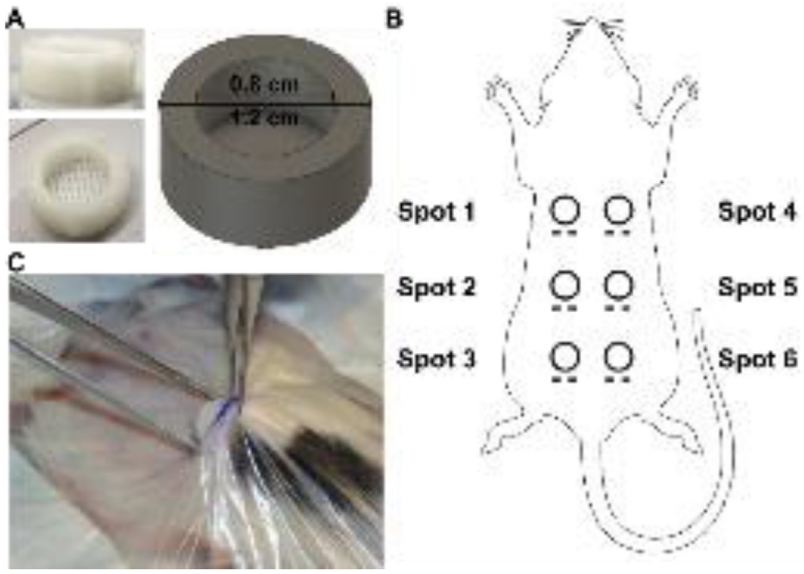

Fig. 1. Subcutaneous model in T cell-deficient athymic rats. A. photograph and 3D render of 3D printed PCL holder used to contain the biomaterials; B. Sample distribution for the subcutaneous model; C. Photograph demonstrating implantation of the PCL holder containing the biomaterial with its open side facing the body.

2.6. In vivo *subcutaneous model*

2.6.1. 3D printing of PCL holders and biomaterial preparation

Polycaprolactone (PCL) holders are printed using RegenHU 3D Discovery® Bioprinter (RegenHU). PCL pellets (MW: 68'413) are melted at 75°C in the heated tank. The printhead is set at 70°C and a stainless steel needle (0.33 mm in diameter) is used with a rate of movement of 4 mm/second and step height between each layer set to 0.26 mm in the Z direction. The following dimensions are used: 0.8 cm inner diameter, 1.2 cm outer diameter and 0.5 cm height (Fig. 1A). PCL sample holders are sterilized using ethylene oxide gas.

For each biomaterial (MeHA, GelMA, fibrin) five groups are created with 6 replicates per group: 1. Biomaterial (Biomaterial only); 2. Biomaterial + cells (MSCs); 3. Biomaterial + cells + 10 mg/mL Dexa-loaded microspheres (MSCs + Dexa); 4. Biomaterial + cells + 30 µg/mL polyP nanoparticles (MSCs + polyP); and 5. Biomaterial + cells + 10 mg/mL Dexa-loaded microspheres + 30 µg/mL polyP (MSCs + Dexa + polyP). The cell encapsulation is carried out just before the implantation according to procedure described in section 2.5.1 and the biomaterials (200 µl) are transferred into the 3D printed PCL holders to constitute the implants for the subcutaneous model.

2.6.2. Animal housing and randomization

A total of 20 skeletally mature (9 – 11-week-old) female T cell-deficient athymic Crl:NIH-*Foxn1*^{rnu} rats (Charles River) with average preoperative weight of 173.4 ± 12.3 g are included in the subcutaneous model study. The rats are randomly allocated to experimental groups and are group-housed in IVC cages (up to 4 rats/cage) with 12 h light/dark cycle. They receive mouse and rat maintenance food and water *ad libitum* and are acclimatized to the housing conditions for at least 2 weeks before surgery. The surgeon and post-op care givers are blinded to group allocation.

2.6.3. Surgical procedure

Rats receive 2 mL pre-warmed Ringer's solution administered subcutaneously before surgery. General anaesthesia is induced and maintained with 6 – 8% and 2 – 3% sevoflurane (Sevoflurane Baxter®, Baxter AG) in 0.6 – 1 L/min oxygen, respectively. Carprofen (5 mg/Kg, Norocarp®, Ufamed AG) and buprenorphine (0.1 mg/Kg, Bupaq®, Streuli Pharma AG) are administered subcutaneously as pre-emptive analgesics.

The animal is placed in ventral recumbency and the back from neck to tail based is aseptically prepared. Incision foil is placed over the back of the animal. Using a dummy PCL sample holder, the positions of the implants are marked onto the skin with a sterile skin marker according to distribution in scheme in Fig. 1B and Supplementary Table 2. The most caudal pockets (Spot 3 and 6) are prepared first, to avoid an implantation above the hips. Next, implants are inserted in spot 2 and 5 and finally in spot 1 and 4. Each incision is done using a scalpel blade no. 15 and it is approximately 2 cm in length. At each incision, a subcutaneous pocket is created bluntly using scissors in cranial direction. The implant is inserted into the subcutaneous pocket with the open side of the PCL holder facing the body (Fig. 1C). The skin is closed by intra cutaneous suturing of the skin (5-0 VICRYL RAPIDE® C-3 reverse cutting, Ethicon).

Paracetamol (Dafalgan Sirup 3%, Bristol Myers Squibb SA) is added to the drinking water (7 mL/100 mL) as analgesic for 4 days post-surgery.

2.6.4. Micro computed tomography

At the end point (8 weeks) general anaesthesia is induced and maintained with 6 – 8% and 2 – 3% Sevoflurane in 0.6 – 1 L/min oxygen, respectively. Animals are euthanized via intracardiac injection of 1 mL Pentobarbital (200 mg/mL). All the implants with the surrounding soft tissue and skin are collected and stored in 4% buffered formalin for imaging. Fixed implants are scanned via micro computed tomography (CT) using VivaCT40 (Scanco Medical AG), as previously described [15]. Briefly, a 10 mm long ROI, with a ø25.6 mm field of view are scanned. The X-ray tube is operated at 70 kV voltage, 114 µA current, with a 0.5 mm aluminium filter. 1000 projections are acquired over 180° rotation, with 200 ms integration time, resulting in a scan time of 21 min.

2.6.5. von Kossa staining

After imaging via microCT, undecalcified sections are obtained after embedding in LR White resin and are stained using von Kossa according to a routine protocol.

2.7. Calvarial defect model

For each biomaterial (MeHA, GelMA and fibrin) four groups are created (all cell-free) with 6 replicates per group: 1. Biomaterial (Biomaterial only); 2. Biomaterial + 10 mg/mL Dexa-loaded microspheres (Dexa); 3. Biomaterial + 30 µg/mL polyP nanoparticles (polyP); and 4. Biomaterial + 10 mg/mL Dexa-loaded microspheres + 30 µg/mL polyP (Dexa+ polyP). The biomaterials are prepared just before the implantation according to procedure described in section 2.5.1. Materials were implanted directly into the defect without a PCL sample holder.

2.7.1. Animal housing

A total of 18 skeletally mature (older than 24-week-old) female, immunocompetent New Zealand white rabbits with average preoperative weight of 3.4 ± 0.2 Kg are included in the calvarial defect model study. During the acclimatization period (8 weeks) the rabbits are group housed with a 12 h dark/ 12 h light cycle, fed with hay, carrots, fennel, parsley, and supplemental feed for rabbits (Biomill) *ad libitum*.

2.7.2. Surgical procedure

Rabbits are sedated with an intramuscular injection of 0.2 mg/Kg medetomodine (Medetor®, Virbac AG), 0.5 mg/Kg midazolam (Dormicum®, Roche) and 0.005 mg/Kg fentanyl (Sintenyl®, Roche) and general anaesthesia is induced with intravenous injection of 0.2 mg/Kg propofol (Propofol 1% MCT®, Fresenius). Animals are placed in sternal recumbency, intubated, and maintained under general anaesthesia with 1.8 – 2.5% sevoflurane in 0.6 – 1 L/min oxygen. As pre-operative analgesic, transdermal fentanyl patches (12 µg/hour, Fentanyl-Mepha®, Mepha Pharma AG) are applied at right ear base and carprofen (4 mg/Kg, Rimadyl®, Pfizer) is administered intravenously. During surgery, fentanyl is administered via constant rate infusion in an ear vein catheter at 30 mcg/kg/h (Fentanyl Sintetica 0.5 mL/10 mL Sintetica SA). The dorsal aspect of the head is clipped and aseptically prepared. A skin incision is made on midline from the nasal bone to the occipital crest using a scalpel blade no. 10 and the occipitalis and temporalis muscles are reflected. A bone cutting jig is placed on the midline, spanning the left and right parietal bones just caudal to the horizontal suture line, and the locations of the four evenly distributed defects are marked through blunt dissections of the periosteum. Following removal of the jig the periosteum of these four locations is further roughened using a scalpel blade no. 15 to help the following engagement of the perforator with the bone. Four craniotomy defects (6 mm diameter) are then created using an Anspach drill (Depuy Synthes) and a 9 mm Codman perforator (Integra Life Science) [16]. Any remaining bone piece is gently removed from the defect site. The biomaterials are press-fit into the defects (Fig. 2A) according to distribution scheme reported in Fig. 2B and Supplementary Table 3. The subcutaneous tissues are closed with a simple interrupted suture pattern (4-0 MONOCRYL, Ethicon), and the skin is closed using 5-0 VICRYL RAPIDE® with an intradermal pattern.

Post-operative analgesia is administered to the animals through subcutaneous injections of 50 µg/Kg buprenorphine (Bupaq®, Streuli Pharma AG) directly after surgery, 6 – 8 h later and the morning of the following day and of 4 mg/Kg Rimadyl® the morning after and then every 24 h for 72 h. Transdermal fentanyl patches are removed at 96 h.

Empty controls (16 samples) are historical data from a previous project [17].

2.7.3. Micro computed tomography

MicroCT scanning is carried out under general anesthesia postoperatively (Day 0) and after euthanasia (6 weeks) using a high resolution peripheral quantitative computed tomography (XTremeCT, Scanco Medical AG) at 82 µm voxel size and using 200 ms integration time. After euthanasia, also a microCT scan (VivaCT40, Scanco Medical AG) is performed at 19 µm voxel size using the following scan parameters: 70 kV, 114 µm and 400 ms integration time.

The standard Scanco segmentation for both scanners is used to segment the samples using Scanco's IPL analysis software (XtremeCT: a Laplace-Hamming filter combined with a global threshold; VivaCT40: a Gaussian filter combined with a global threshold). Postoperative and subsequent scans are overlaid using in Amira 2019.4 (Thermo Fisher Scientific, USA) and a cylinder of 6 mm diameter are placed in the defect site. The bone volume (BV) in the cylinder is calculated in both scans. New bone volume fraction is calculated as $BV/TV = (BV_{euthanasia} - BV_{postoperatively})/TV$, where the total volume (TV) of the defect was calculated as a cylinder of 6mm diameter (defect size) with an estimated thickness of 1.5 mm.

2.7.4. Semi-quantitative histopathological evaluation

Following euthanasia with an overdose of pentobarbital, the calvaria containing the 4 defects is resected from the skull using an oscillating saw and it is stored in 4% buffered formalin for histological processing. Undecalcified sections are obtained after embedding in methylmethacrylate and are stained using Giemsa-Eosin according to a routine protocol. Histopathological severity is assessed using a 6-point grading scheme (0 – 5). Among others, semi-quantitative analysis is focused on new bone formation, namely the defect closure, which can be characterized by two parameters: 1) the size (μm^2) of the defect area filled with new bone tissue; and 2) the distance (µm) of the defect diameter spanned by bone tissue. Additionally, parameters characterizing the biomaterial itself (amount, surface irregularity, fragmentation, pores), its relationship towards the host tissue (cell infiltration, osseous integration, mineralization) and its capacity to induce inflammatory cell reactions (granulocytic, lymphocytic, granulomatous, fibrotic capsule formation) are analyzed. Finally, unintended changes of the adjacent brain tissue (hemosiderin deposition, astrocytosis, prolapse of brain tissue and nests of meningeal tissue in the defect, biomaterial in the brain) are also recorded.

2.8. Statistical analyses

Normally distributed data is assessed using one way ANOVA, with Tukey's multiple comparison test. Semiquantiative data is assessed using Kruskal-Wallis. Data is analyzed in GraphPad Prism 8 software (GraphPad Software, San Diego, CA, USA) $p < 0.05$ being considered significant.

3. Results

3.1. In vitro release of dexamethasone from PCL microspheres

The PCL microspheres are produced with an efficiency of Dexa encapsulation of 51.37% ± 14.71, which corresponds to 99.5 µmol and 0.678 µmol per mg of PCL. The quantification via HPLC shows a 35% of Dexa release over a period of 500 h with over 15% Dexa being released in the first 48 h (Fig. 3A). Cumulative drug release of Dexa is fitted using the conventional model Korsmeyer-Peppas, which is defined as $K_{kp}*t\hat{}n$, K_{kp} being the release constant, t the time and n the slope as described previously [10]. Dexa drug release can be plotted as logarithmic scale: linear trendlines with $R^2 = 0.979$, $n = 0.313$ and $R^2 = 0.955$, $n = 0.2972$ for the release of the total amount of Dexa and the percentage, respectively, indicating a purely diffusion-based drug release with negligible effects of polymer erosion (Fig. 3B).

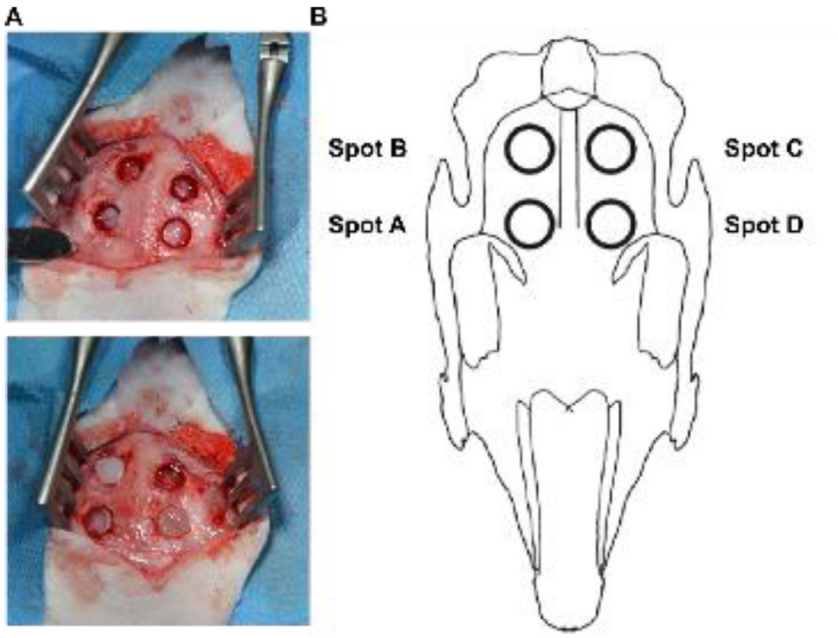

Fig. 2. Calvarial defect model in New Zealand white rabbits. A. Photograph showing the defects soon after creation (upper row) and after material implantation (lower row); B. Sample distribution for the calvarial defect model.

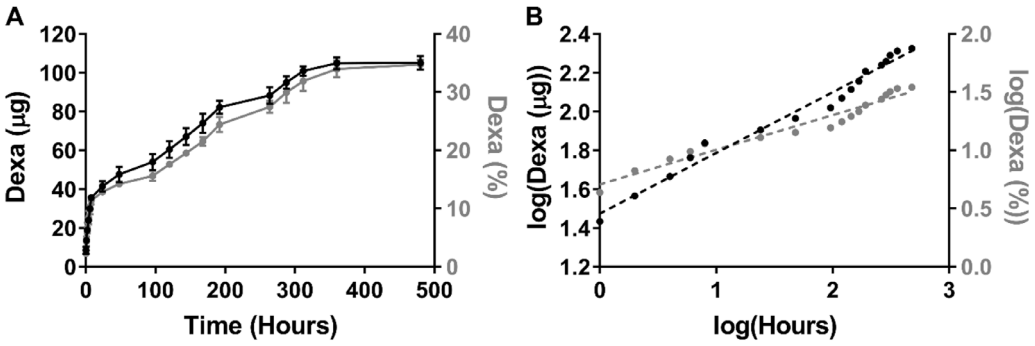

Fig. 3. *In vitro* release of Dexa from PCL microspheres. A) The release of Dexa from PCL microspheres is measured *in vitro* up to 500 h and expressed as total amount (µg) and percentage of encapsulated Dexa. Data are shown as mean ± S.D. of three independent batches; B) Dexa release remodelled to fit the Korsmayer-Peppas model for sustained drug release.

3.2. Gene expression profile of BM-MSCs under osteogenic culture conditions

The differentiation of BM-MSCs into osteoblasts is characterized by the gene expression of specific transcription factors and mineralization associated markers. For this reason, we studied the expression of the transcription factors *Runx2, Sox9, Runx2/Sox9* ratio [18], *PPARγ* and *Sp7*, and alkaline phosphatase (*ALPL*) and integrin binding sialoprotein *(IBSP*) as proteins involved in the mineralization process (Fig. 4). The addition of Dexa downregulates the expression of *Runx2, Sox9* and *PPARγ* in MeMA, but upregulates the *Runx2/Sox9* ratio and *ALPL*. Gene expression values in GelMA is unchanged when Dexa is added, except for *ALPL*. Dexa causes a high upregulation of *ALPL* in Fibrin, an upregulation in *Runx2* and the *Runx2/Sox9* ratio and a downregulation in *PPARγ*. The addition of Dexa to all three biomaterials upregulates the expression of *ALPL*, which is not the case when Dexa is combined with polyP, or polyP alone. The addition of polyP causes downregulation in *ALPL* in all biomaterials and in *PPARγ* in MeHa and Fibrin, an upregulation of *Sox9* in all biomaterials or stays unchanged in the other groups. The combination of both bioactive factors does not follow the trend of each factor individually, but increases the *Runx2/Sox9* ratio in GelMA and polyP. Each of the bioactive factors and in combination leads to a downregulation of the *PPARγ* gene in MeHA and fibrin, but not in GelMA.

3.3. In vitro osteogenic differentiation is confirmed by von Kossa staining and gene expression of markers associated to mineralization

All three tested cell-laden biomaterials with or without the addtion of Dexa and/or polyP show promising osteogenic poential, indicated by positive von Kossa staining (Fig. 5A) and upregulation of osteogenically-relevant gene expression markers IBSP and SP7 (Fig. 5B). No osteogenic response was detected in biomateral only (Supplementary Fig. 3). The osteogenic response is enhanced when Dexa is added to GelMA and Fibrin, or when polyP is added to MeHA, demonstrated by increased mineral deposition seen in the von Kossa images and upregulation of the IBSP and SP7 genes. The addition of polyP in fibrin with and without Dexa shows increased mineralization, but does not correlate to the gene expression profile, likely due to artifacts, which could be caused by the shrink-

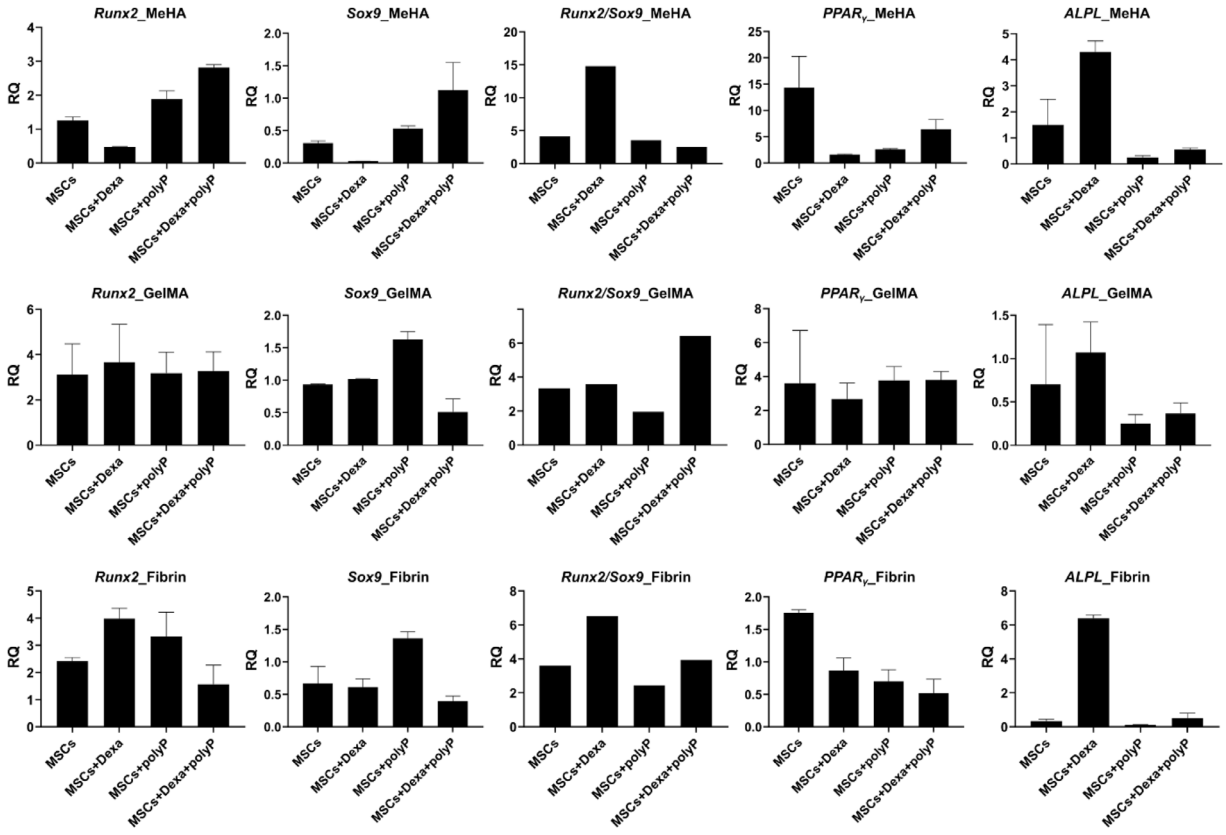

Fig. 4. *In vitro* gene expression profile of BM-MSCs under osteogenic culture conditions within different biomaterials. Relative quantification (RQ) at day 28 calculated using the $2^{-\Delta\Delta Ct}$ formula with *RPLP0* as reference gene and sample at day 0 as calibrator. All the data are shown as mean± SEM of three replicates. *Runx2*: Runt related transcription factor 2; *SOX9*: SRY-Box transcription factor; *ALPL*: Alkaline phosphatase, biomineralization associated; *PPARγ*: peroxisome proliferator activated receptor gamma; *RPLP0*: ribosomal protein lateral stalk subunit P0.

Table 2
Overview of sample allocation for surgery 1 of subcutaneous implantation in nude rats.

Rat #	Spot 1	Spot 2	Spot 3	Spot 4	Spot 5	Spot 6
218001	MeHA	GelMA	N/A	Fibrin	PCL only	N/A
218002	MeHA*	GelMA	N/A	Fibrin	PCL only	N/A
218003	MeHA*	GelMA	N/A	Fibrin	PCL only	N/A
218004	MeHA+MSC	GelMA+MSC	Fibrin+MSC	MeHA+MSC+Dexa*	GelMA+MSC+Dexa	Fibrin+MSC+Dexa
218005	MeHA+MSC	GelMA+MSC	Fibrin+MSC	MeHA+MSC+Dexa*	GelMA+MSC+Dexa	Fibrin+MSC+Dexa
218006	MeHA+MSC	GelMA+MSC	Fibrin+MSC	MeHA+MSC+Dexa	GelMA+MSC+Dexa	Fibrin+MSC+Dexa
218007	MeHA+MSC+polyP	GelMA+MSC+polyP	Fibrin+MSC+polyP	MeHA+MSCs+Dexa+polyP*	GelMA+MSC+Dexa+polyP	Fibrin+MSC+Dexa+polyP
218008	MeHA+MSC+polyP	GelMA+MSC+polyP	Fibrin+MSC+polyP	MeHA+MSCs+Dexa+polyP	GelMA+MSC+Dexa+polyP	Fibrin+MSC+Dexa+polyP
218009	MeHA+MSC+polyP*	GelMA+MSC+polyP	Fibrin+MSC+polyP	MeHA+MSCs+Dexa+polyP*	GelMA+MSC+Dexa+polyP	Fibrin+MSC+Dexa+polyP

* Gel broke while implanting (n=7/15 MeHA samples); **in bold** animals euthanized at day 4, before endpoint, due to severe weight loss (n=3/9 animals); *in italics* animals with severe weight loss but not sufficient for exclusion (n=3/9 animals).

age behaviour of fibrin, making fibrin the least stable biomaterial used.

All materials were then tested *in vivo* in a subcutaneous implantation model in nude rats.

3.4. Subcutaneous model in nude rats

The subcutaneous surgery was performed in two sessions: surgery 1 included nine animals (6 samples per animal), of which one animal (Animal #218011) was lost before the surgery (Table 2) and surgery 2 included ten animals (6 samples per animal) (Table 3). Both tables include notes about deviations. An overview of the initial body weight loss of surgery 1 and 2 is shown in Supplementary Fig. 4 and Supplementary Fig. 5, respectively. Based on the body weight loss observed in surgery 1, surgery 2 focused on the comparison between the effects of the cells and the effect of Dexa inclusion. The overall substantial body weight loss is caused by a systemic response triggered by the implantation of the biomaterials. Three and two animals from surgery 1 and 2, respectively, were excluded due to severe weight lost (highlighted as bold in Table 2 and Table 3). Implanted biomaterials with and without bioactive factors did not produce consistent mineralization, as no ectopic mineralization was detected based on von Kossa staining of histology slides (Supplementary Fig. 6A). MeHA combined with Dexa and polyP showed moderate mineralization as determined by MicroCT images and von Kossa staining (Supplementary Fig. 6B). Subsequently, all the samples were then assessed in the orthotopic calvarial defect model in rabbits.

3.5. Calvarial defect model in rabbit

The calvaria surgery was performed in three repetitions, with 6 animals per biomaterial in each repetition (4 samples per animal), with notes about deviations (Table 4). Data was compared to

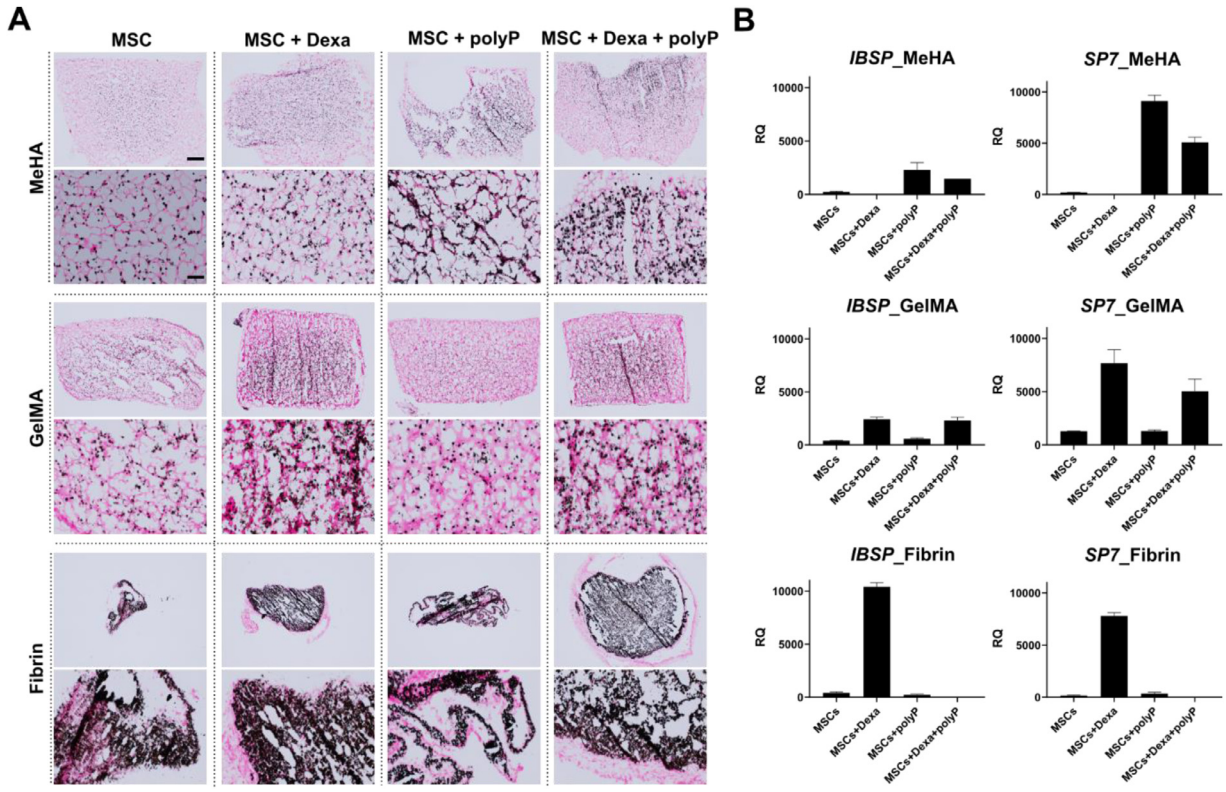

Fig. 5. von Kossa staining and gene expression of markers associated to late *in vitro* mineralization. A. Representative images of von Kossa staining at day 28. Scale bars are 500 and 100 µm for the low and high magnification, respectively; B. Relative quantification (RQ) at day 28 calculated using the $2^{-\Delta\Delta Ct}$ formula with *RPLP0* as reference gene and sample at day 0 as calibrator. All the data are showed as mean± SEM of three replicates. *IBSP*: integrin binding sialoprotein; *SP7*: Sp7 transcription factor; *RPLP0*: ribosomal protein lateral stalk subunit P0.

Table 3
Overview of sample allocation for surgery 2 of subcutaneous implantation in nude rats.

Rat #	Spot 1	Spot 2	Spot 3	Spot 4	Spot 5	Spot 6
218010	MeHA+MSC	GelMA+MSC	Fibrin+MSC	MeHA+MSC*	GelMA+MSC	Fibrin+MSC
218016**	MeHA+MSC	GelMA+MSC	Fibrin+MSC	MeHA+MSC	GelMA+MSC	Fibrin+MSC
218012	MeHA+MSC	GelMA+MSC	Fibrin+MSC	MeHA+MSC*	GelMA+MSC	Fibrin+MSC
218013	MeHA	GelMA	Fibrin	MeHA+Dexa*	GelMA+Dexa	Fibrin+Dexa
218014	MeHA	GelMA	Fibrin	MeHA+Dexa	GelMA+Dexa	Fibrin+Dexa
218015	MeHA	GelMA	Fibrin	MeHA+Dexa	GelMA+Dexa	Fibrin+Dexa
218017	MeHA+polyP	GelMA+polyP	Fibrin+polyP	MeHA+Dexa+polyP*	GelMA+Dexa+ polyP	Fibrin+Dexa+polyP
218018	MeHA+polyP*	GelMA+polyP	Fibrin+polyP	MeHA+Dexa+polyP*	GelMA+Dexa+ polyP	Fibrin+Dexa+polyP
218019	MeHA+MSC	GelMA+MSC	Fibrin+MSC	MeHA+MSC+Dexa*	GelMAMSC+ Dexa	Fibrin+MSC+Dexa
218020	MeHA+MSC*	GelMA+MSC	Fibrin+MSC	MeHA+MSC+Dexa*	GelMA+MSC+ Dexa	Fibrin+MSC+Dexa

* Gel broke while implanting (n=8/20 MeHA samples).
** Animal replaced 218011 excluded due to a rash; **in bold** animals euthanized at day 5, before endpoint, due to severe weight loss (n=2/10 animals); In italic animals with severe weight loss but not enough for exclusion (n=4/10 animals); Underlined are animals that did not recover from anaesthesia (n=1/10 animals). **in bold** animals euthanized at day 4, before endpoint, due to severe weight loss (n=3/9 animals); *in italics* animals with severe weight loss but not sufficient for exclusion (n=3/9 animals).

historical empty controls of previously published work using the same model system [17] in line with 3R principles. BV/TV values based on CT scanning and semiquantitative histopathological analysis correlate in terms of bone repair of the empty defect and the biomaterials with and without bioactive factors after 6 weeks of implantation (Fig. 6). Representative microCT images are presented in supplementary Fig. 7. The empty defect shows slightly improved bone regeneration compared to the other groups. The implantation of biomaterials with and without the addition of bioactive factors did not improve the bone regeneration outcome and the defect remained without mineralization. Histology images independent of the treatment show that gap closure for all tested biomaterials is by areas of newly formed trabecular bone (stained rose) is generally quite low and is only visible at the periphery of the osteotomy edges (Fig. 7). Masson's trichrome images are presented in supplementary Fig. 8. In some spots a thin layer of bone at the meningeal/inner side of the defect leads to partial defect bridging (least pronounced in GelMA, highest in Empty; in biomaterial-treated spots a complete bridging was never observed). Direct contact of bone to biomaterial (osseous integration) was nearly absent and only recorded in very few spots for very short distances. MeHA (stained light blue to blue) displays pronounced fragmentation, indicating a certain fragility of this biomaterial and cell infiltration is dramatically limited to only superficial areas (Table 5) investigated via a blinded semiquantitative scoring system. MeHA also displays low amounts of inflammatory cell infiltrates (lymphocytic

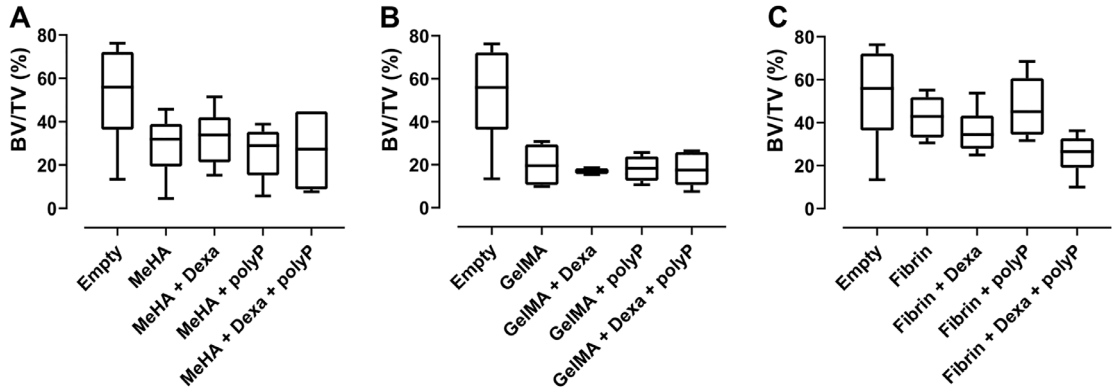

Fig. 6. Bone volume fraction for calvarial defect model in rabbit. Ratios of bone volume (BV) and total volume (TV) post euthanasia (6 weeks post-surgery) are calculated based on XtremeCT post-euthanasia (6 weeks post injury).

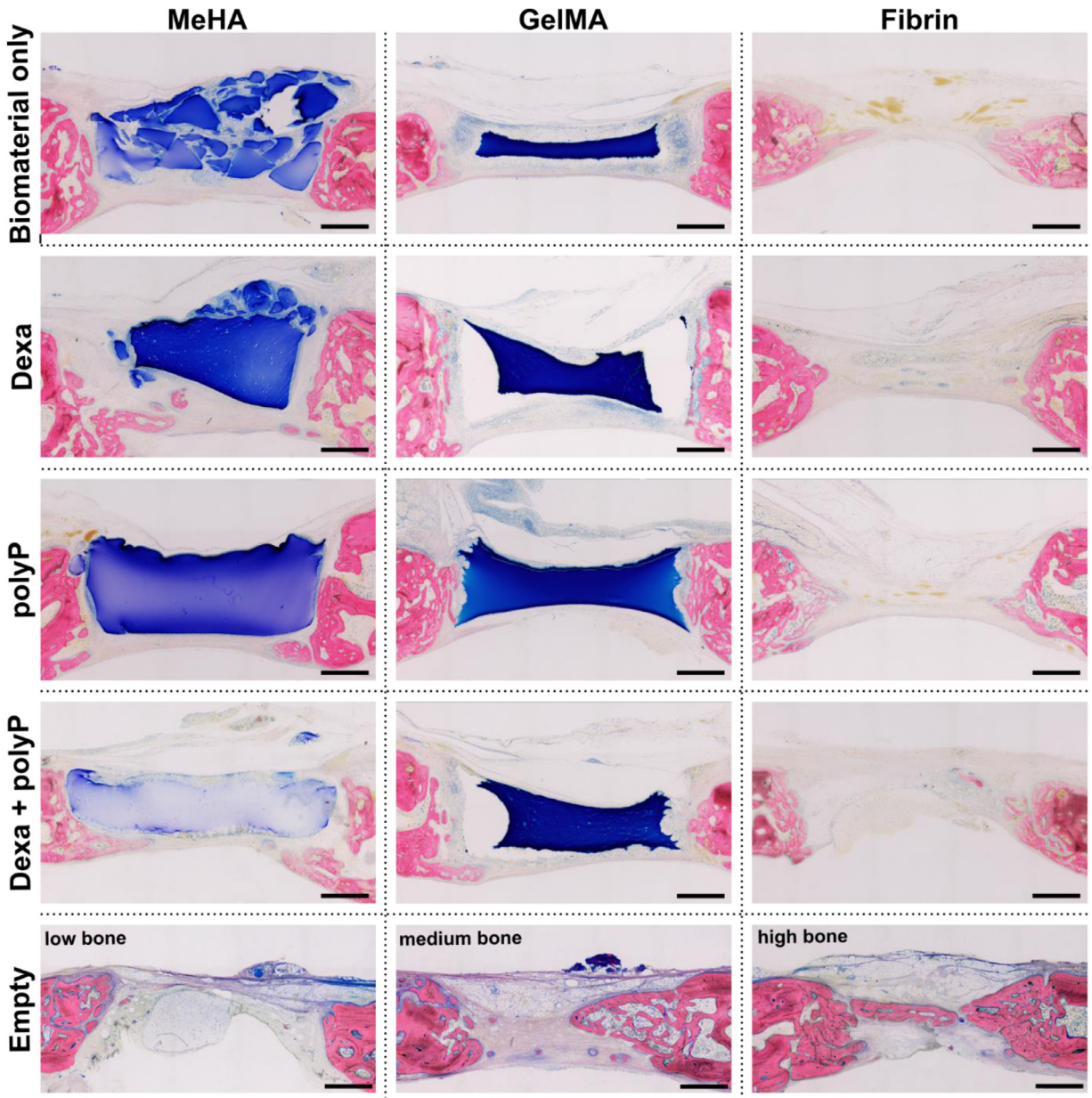

Fig. 7. (calvarial defect model in rabbit). Histopathological changes in representative calvarial defects in rabbit for each treatment group (6 weeks post surgery; Giemsa Eosin stained, MMA-embedded thick-sections). The representative images show the inter-animal variability of empty spots. Overall, the median amount of bone is higher than that of the 3 biomaterials. Scale bars are 1 mm.

Table 4
Overview of surgery results (calvarial defect model in rabbit).

Rabbit #	Spot A	Spot B	Spot C	Spot D
319068	Fibrin	MeHA+Dexa	GelMA+polyP	Fibrin±Dexa±polyP
319069	**Fibrin**	MeHA+Dexa	GelMA+polyP	**Fibrin±Dexa±polyP**
319073	Fibrin	***MeHA+Dexa***	GelMA+polyP	**Fibrin+Dexa+polyP**
319079	Fibrin	MeHA+Dexa	**GelMA±polyP**	**Fibrin+Dexa+polyP**
319080	Fibrin	**MeHA±Dexa**	*GelMA+polyP*	**Fibrin+Dexa+polyP**
319086	Fibrin	MeHA+Dexa	*GelMA±polyP*	***Fibrin+Dexa+polyP***
319070	MeHA	**GelMA±Dexa**	Fibrin+polyP	**MeHA+Dexa+polyP**
319074	MeHA	GelMA+Dexa	**Fibrin±polyP**	MeHA+Dexa+polyP
319075	MeHA	GelMA±Dexa	Fibrin+polyP	MeHA+Dexa+polyP
319076	MeHA	GelMA+Dexa	Fibrin±polyP	*MeHA+Dexa+polyP*
319081	**MeHA**	**GelMA±Dexa**	**Fibrin+polyP**	**MeHA+Dexa+polyP**
319082	MeHA	**GelMA+Dexa**	**Fibrin+polyP**	MeHA+Dexa+polyP
319071	**GelMA**	**Fibrin+Dexa**	MeHA+polyP	**GelMA+Dexa+polyP**
319077	GelMA	**Fibrin±Dexa**	*MeHA±polyP*	GelMA+Dexa+polyP
319078	GelMA	**Fibrin+Dexa**	MeHA+polyP	GelMA+Dexa+polyP
319083	GelMA	**Fibrin+Dexa**	*MeHA+polyP*	***GelMA+Dexa+polyP***
319084	GelMA	**Fibrin±Dexa**	**MeHA±polyP**	GelMA+Dexa+polyP
319085	**GelMA**	**Fibrin±Dexa**	**MeHA+polyP**	GelMA+Dexa+polyP

Grey: animals with macroscopic *dura mater* injury defined by surgery observation in at least one spot (n 13/34); underlined: spots with macroscopically altered/intact/not attached dura mater defined by surgery observation (n=18/88); **bold**: spots with microscopic dura mater injury (n= 43/88 spots; defined by presence of meningeal tissue nests in defect); italic: spots with hydrogel not fitting well into the defect (n 8/72 treated spots).

Table 5
Results of semiquantitative histopathological analysis of the calvarial defects.

Parameter	MeHA	GelMA	Fibrin	Empty
Number of samples (n)	23*	23**	24	16
Bone tissue				
Defect closure, bone, area	1.7	1.3	2.2	2.3
Defect bridging, bone, span/length	2.0	1.7	2.6	3.0
Biomaterial properties				
Amount, blue material	3.6****	3.6	1.4***	1.0***
Surface irregularity, hydrogel	1.4	2.4	1.5***	0.0
Fragmentation, hydrogel	2.2*****	0.7	2.8***	1.0***
Pores, hydrogel	1.7	1.9	1.2***	0.0
Host tissue reaction				
Cell infiltration, into biomaterial	0.9	0.5	0.4***	0.0
Osseous integration of biomaterial	0.7	0.3	0.0	0.0
Mineralization of biomaterial	0.0	0.3	0.0	0.0
Inflammatory reaction				
Inflammation, granulocytic/purulent	0.2	0.0	0.0	0.0
Inflammation, lymphocytic	1.6	3.0	2.0	0.3
Inflammation, granulomatous	1.0	2.2	1.1	0.1
Fibrosis (e.g. capsule formation)	2.2	1.3	1.0***	1.3

* 1 Sample of MeHA was excluded due loss of gel during post-mortem handling.
** 1 Sample of GelMA was excluded due to loss of gel during post-mortem handling.
*** Values compromised/too high (spill-over of MeHA into neighbouring fibrin-treated or empty spot, n= 21/39 defects).
**** Value compromised/too low (spill-over of MeHA- into neighbouring spots, n=9/39 defects).
***** Value compromised/too high (due to damage/fragmentation during surgery, n=9/39 defects).

and granulomatous in nature), with a low tendency for a fibrous encapsulation.

In contrast to MeHA, GelMA (stained dark blue) displays nearly no fragmentation but a pronounced tendency to shrink. Similarly, cell infiltration was nearly absent in GelMA constructs. Compared to MeHA, the inflammatory cell infiltrates (both lymphocytic and granulomatous) are more pronounced in GelMA, reaching moderate amounts. In contrast, the tendency to form a fibrotic capsule is lower.

Fibrin constructs are observed to be completely resorbed by 6 weeks post-surgery, with increased evidence of partial bridging when compared to MeHA and GelMA biomaterials. Inflammatory cell infiltration (lymphocytic and granulomatous) is low to low and comparable with MeHA.

4. Discussion

Bone is a complex tissue and is characterized by constant remodelling that occurs throughout life. Healthy bone is extremely tough and resilient and has incredible self-healing potential leaving a regenerated defect without scars. With the current lifestyle changes and increasing aging population, combined with the diminished bone healing capacity in elderly patients, suggests that healing complications associated with bone fractures (e.g., delayed bone healing and potential progression to non-union) are estimated to rise [19,20]. The current standard of care, which involves bone grafting from autologous tissue or allografts, as well as implantation of BMP-2-laden collagen sponges, are associated with significant drawbacks [21], thus necessitating a search for alternative bone regenerative biomaterials. A tissue engineered scaffold can provide a new alternative solution but, despite extensive research, recent advances in this field show a low clinical translation rate, potentially due the complexity of the tissue engineering approach but also due to the methods typically used to screen potential therapies. The reproducibility and reliability of any research study is based on the robustness of the methods and is negatively affected when insufficient information and details are provided. In the case of animal studies, the consequence is not only a lack of reproducibility and reliability but most importantly the resulting experimental animals being wasted. Therefore, for science and ethics it is crucial to fully report on animal data using reporting structures such as the ARRIVE guidelines 2.0 [22].

The combination of cells, biomaterials and factors are difficult to assess using only simple *in vitro* tests, and preclinical models need to be more robustly chosen to answer the question at hand. In this study we sought to assess the performance of a variety of tissue engineering relevant biomaterials both *in vitro* and in two preclinical models commonly used to assess efficacy: an ectopic rodent subcutaneous implant model and a rabbit calvarial defect model. We adopted the typical workflow of a biomaterial-based research study including the design, conduct and analysis and will discuss common pitfalls.

Within this study we chose materials that have generated positive *in vitro* results and used bioactive factors with known *in vitro* and *in vivo* osteogenic potential. Dexamethasone is a routinely used osteogenic and chondrogenic *in vitro* supplement [23], which has also shown benefits in clinical bone regeneration [24]. PolyP is an inorganic energy source with strong wound healing [25] and osteoinductive potential both *in vitro* and *in vivo,* including in calvarial models [26,27]. The presented results showed promising osteogenic potential of MSCs-laden biomaterials (MeHA, GelMA, fibrin) in combination with bioactive factors (Dexa-MP, polyP NP) *in vitro*, based on gene expression of relevant markers and von Kossa staining. The cell concentration within the biomaterials is based on a previous work [28].

When studying new bone biomaterials, promising *in vitro* results often do not correlate with the outcome obtained from the *in vivo* experiments. While this is anecdotally discussed, there are very few papers that directly address this issue [9]. Thus, there is a need to investigate this discrepancy further and use the data obtained to improve the process used to test next generation bone biomaterials. Why *in vitro* data leads to false positive results are still largely unknown and yet it is a major weakness in the material development pathway.

Therefore, a particular focus must be placed on the limitations of each assay utilized. *In vitro* assays typically use only one cell type and use a classical dexamethasone containing os-

teogenic medium [8,29]. However, bone can heal via two different routes, either intramembranous bone formation, where the infiltrating cells differentiate directly into an osteoblast phenotype, or endochondral ossification, which utilizes an initial cartilage template formed as a result of chondrogenic differentiation of callus-infiltrating MSCs, which subsequently mineralizes into bone tissue. These two pathways require different conditions, both in the scaffold design and the *in vitro* culture media used [1]. Therefore, it should also be considered whether osteogenic medium should be the standard when testing materials where the endochondral route is expected to be the primary mechanism of action. While these are the classically accepted pathways, evidence is emerging that the actual process of fracture repair and bone formation may be more complex [30,31]. This should also be considered when designing the testing protocol for new materials. A further consideration is whether the planned clinical use would include cell encapsulation and delivery, or whether a cell-free material will be implanted with subsequent cell infiltration. Effective testing of these conditions *in vitro* will require a source of cells capable of undergoing differentiation. While the initial *in vitro* tests will require cells being encapsulated and differentiation assessed, an additional cell migration assay would be warranted when the final implanted material is planned to be used in a cell free approach and therefore requires cell infiltration.

Within this study, each material demonstrated *in vitro* osteogenic differentiation of encapsulated hMSCs with various degrees of success. Yet cell free orthotopic implantation suggested there was limited cell infiltration, leading to no intramembranous bone formation. The materials used in this study have been utilized in various bone healing studies and each has a range of potential permutations in formulation (e.g. crosslinking and resulting mechanical properties). The need for cell migration and the effect of each modification on the ability of cells to enter the gel should also be considered and reported during the initial material assessments.

As the *in vitro* work showed promise, all materials were tested using encapsulated hMSCs in a nude rat subcutaneous model. In our data, subcutaneous implantation of MSC-laden biomaterials did not lead to ectopic mineralization, despite the presence of osteogenic cells and osteogenic induction signals, a situation similar to the *in vitro* study where mineralization occurred. Given the inherent inter-donor variability in osteogenic and chondrogenic potential of human MSCs, we used the same donor for both the *in vitro* and *in vivo* experiments to avoid donor-specific differences. The reasons for the poor correlation of *in vitro* and *in vivo* outcomes are unclear, with potential off target effects or doses of bioactive factors. Previous studies have demonstrated ectopic bone formation using subcutaneous implantation, where a common theme is the incorporation of an osteoinductive component such as BMP-2 or demineralized bone that drives the osteogenic response [32–34]. This suggests that the subcutaneous model requires the implantation of all the required differentiation drivers. The implantation of cell-laden biomaterials in nude mice is an established procedure, however, when using human cells in a nude rat model, it should not be overlooked that although they lack T cells, the Crl:NIH-*Foxn1rnu* rats have a normal complement of B and NK cells, which may still respond to the xenogeneic cells. MSCs have immunosuppressive potential [35,36], but their implantation within immunocompromised animal models may diminish the translational aspect, due to the importance of the immune system for optimal bone healing. Initial inflammation is beneficial for bone healing [37], but maintained inflammation impairs healing [38]. A way to potentially improve efficacy testing of hMSC - laden biomaterials and its clinical translation is the use of humanized mice engrafted with functional human cells [39]. Bone healing has been shown to be dependent on the immune status of the animal by implanting MSC-laden alginate hydrogels into T cell-deficient nude rats and comparing the response to immunocompetent rats [40]. Nude rats display improved healing response in muscle tissue compared to competent rats, indicating an incomplete understanding how animal models respond when biomaterials are applied [41].

To establish the role on the *in vivo* model in data interpretation, all materials were then tested cell-free within an intramembranous orthotopic calvarial defect model in immunocompetent animals. The implanted material led to a reduced bone formation when compared to the empty defect, with the difference being more extreme in the MeHA and GelMA groups, while the bone formation using fibrin was similar in volume. The histological evaluation supported this conclusion and indicated this was due to a lack of cell migration into the defect, further highlighting the critical role on a migration assay in the materials development algorithm. Furthermore, dexa-laden biomaterials did not enhance calvarial bone repair compared to the empty defect. Other publications using these biomaterials implanted in calvarial defect reported positive data [42–48], which indicates the exact formulation is key to the response obtained [49].

This raises questions regarding the workflow that should be adopted when testing new materials for osteogenic differentiation. Taken together it suggests improvements can be made to the bone testing algorithm. We would suggest routine use of a migration assay, humanized rodent models to allow the use of human cells, and *in vitro* challenge of the materials with immune cells to assess unwanted inflammatory responses. One key change could be the implantation of proposed materials into an orthotopic model, such as a drill hole model, early in the development cycle. This would identify failures at an early time point, allowing optimization to be focused on materials that have already shown potential in an orthotopic environment. Due to the increasing evidence of immunological regulation of healing, this should ideally be done in an immune competent animal to identify early any unexpected reactions. Substantial effort is often placed into optimizing *in vitro* osteogenesis when there is no guarantee this will reflect the final orthotopic function. An early orthotopic screen *in vivo* would highlight which materials offer true potential thus reducing the effort placed to test materials *in vitro* that are destined to fail *in vivo*. Furthermore, the adequacy of the *in vivo* model in assessing complex TE approaches, and how to ask the right question with the right model (e.g. direct *versus* indirect bone formation) when using combinations of cells, bioactive factors and biomaterials while also applying the 3Rs, must not be overlooked.

In conclusion, despite promising *in vitro* data, 12 material combinations utilizing 3 different base materials all failed to lead to bone formation in an orthotopic model. Optimization of *in vitro* material testing protocols may identify some of these failures at an earlier time point and more studies are needed to understand how host responses to biomaterials differ based on the animal model used.

Declaration of Competing Interest

The authors declare that there is no conflict of interest.

Funding

This study is funded by the AO CMF.

Acknowledgements

The authors would like to thank Mr. Flavio Linardi for the MeHA and GelMA synthesis and the staff of the preclinical and histology

facility of the AO Research Institute Davos for the animal surgeries and the histological preparation.

Supplementary materials

Supplementary material associated with this article can be found, in the online version, at doi:10.1016/j.actbio.2022.08.021.

References

[1] A.R. Armiento, L.P. Hatt, G. Sanchez Rosenberg, K. Thompson, M.J. Stoddart, Functional biomaterials for bone regeneration: a lesson in complex biology, Adv. Funct. Mater. 30 (44) (2020) 1909874.

[2] N. Jaiswal, S.E. Haynesworth, A.I. Caplan, S.P. Bruder, Osteogenic differentiation of purified, culture-expanded human mesenchymal stem cells in vitro, J. Cell. Biochem. 64 (2) (1997) 295–312.

[3] J.P. Cassella, N. Garrington, T.C. Stamp, S.Y. Ali, An electron probe X-ray microanalytical study of bone mineral in osteogenesis imperfecta, Calcif. Tissue Int. 56 (2) (1995) 118–122.

[4] L.M. Schäck, S. Noack, R. Winkler, G. Wißmann, P. Behrens, M. Wellmann, M. Jagodzinski, C. Krettek, A. Hoffmann, The phosphate source influences gene expression and quality of mineralization during in vitro osteogenic differentiation of human mesenchymal stem cells, PLoS One 8 (6) (2013) e65943-e65943.

[5] L. Phelipe Hatt, K. Thompson, W.E.G. Müller, M.J. Stoddart, A.R. Armiento, Calcium polyphosphate nanoparticles act as an effective inorganic phosphate source during osteogenic differentiation of human mesenchymal stem cells, Int. J. Mol. Sci. 20 (22) (2019).

[6] W.E.G. Müller, M. Neufurth, S. Wang, M. Ackermann, R. Muñoz-Espí, Q. Feng, Q. Lu, H.C. Schröder, X. Wang, Amorphous, smart, and bioinspired polyphosphate nano/microparticles: a biomaterial for regeneration and repair of osteo-articular impairments in-situ, Int. J. Mol. Sci. 19 (2) (2018).

[7] J.M. Seong, B.C. Kim, J.H. Park, I.K. Kwon, A. Mantalaris, Y.S. Hwang, Stem cells in bone tissue engineering, Biomed. Mater. 5 (6) (2010) 062001.

[8] S. Walsh, G.R. Jordan, C. Jefferiss, K. Stewart, J.N. Beresford, High concentrations of dexamethasone suppress the proliferation but not the differentiation or further maturation of human osteoblast precursors in vitro: relevance to glucocorticoid-induced osteoporosis, Rheumatology 40 (1) (2001) 74–83.

[9] G. Hulsart-Billström, J.I. Dawson, S. Hofmann, R. Müller, M.J. Stoddart, M. Alini, H. Redl, A. El Haj, R. Brown, V. Salih, J. Hilborn, S. Larsson, R.O. Oreffo, A surprisingly poor correlation between in vitro and in vivo testing of biomaterials for bone regeneration: results of a multicentre analysis, Eur. Cell Mater. 31 (2016) 312–322.

[10] S.G. Rotman, K. Thompson, D.W. Grijpma, R.G. Richards, T.F. Moriarty, D. Eglin, O. Guillaume, Development of bone seeker–functionalised microspheres as a targeted local antibiotic delivery system for bone infections, J. Orthop. Transl. 21 (2020) 136–145.

[11] J.A. Burdick, C. Chung, X. Jia, M.A. Randolph, R. Langer, Controlled degradation and mechanical behavior of photopolymerized hyaluronic acid networks, Biomacromolecules 6 (1) (2005) 386–391.

[12] A.I. Van Den Bulcke, B. Bogdanov, N. De Rooze, E.H. Schacht, M. Cornelissen, H. Berghmans, Structural and rheological properties of methacrylamide modified gelatin hydrogels, Biomacromolecules 1 (1) (2000) 31–38.

[13] O.F. Gardner, M. Alini, M.J. Stoddart, Mesenchymal stem cells derived from human bone marrow, Methods Mol. Biol. 1340 (2015) 41–52.

[14] J. Hasler, L.P. Hatt, M.J. Stoddart, A.R. Armiento, Stable reference genes for qPCR analysis in BM-MSCs undergoing osteogenic differentiation within 3D hyaluronan-based hydrogels, Int. J. Mol. Sci. 21 (23) (2020).

[15] V.A. Stadelmann, K. Thompson, S. Zeiter, K. Camenisch, U. Styger, S. Patrick, A. McDowell, D. Nehrbass, R.G. Richards, T.F. Moriarty, Longitudinal time-lapse in vivo micro-CT reveals differential patterns of peri-implant bone changes after subclinical bacterial infection in a rat model, Sci. Rep. 10 (1) (2020) 20901.

[16] O. Guillaume, T. Schmid, K. Kluge, F.E. Weber, R.G. Richards, U. Eberli, D. Eglin, S. Zeiter, Introduction of the Anspach drill as a novel surgical driller for creating calvarial defects in animal models, J. Orthop. Res. 37 (5) (2019) 1183–1191.

[17] O. Guillaume, M.A. Geven, C.M. Sprecher, V.A. Stadelmann, D.W. Grijpma, T.T. Tang, L. Qin, Y. Lai, M. Alini, J.D. de Bruijn, H. Yuan, R.G. Richards, D. Eglin, Surface-enrichment with hydroxyapatite nanoparticles in stereolithography–fabricated composite polymer scaffolds promotes bone repair, Acta Biomater. 54 (2017) 386–398.

[18] C. Loebel, E.M. Czekanska, M. Bruderer, G. Salzmann, M. Alini, M.J. Stoddart, In vitro osteogenic potential of human mesenchymal stem cells is predicted by Runx2/Sox9 ratio, Tissue Eng. Part A 21 (1-2) (2015) 115–123.

[19] C. Zhang, J. Feng, S. Wang, P. Gao, L. Xu, J. Zhu, J. Jia, L. Liu, G. Liu, J. Wang, S. Zhan, C. Song, Incidence of and trends in hip fracture among adults in urban China: a nationwide retrospective cohort study, PLoS Med. 17 (8) (2020) e1003180.

[20] G. Adami, A. Fassio, D. Gatti, O. Viapiana, C. Benini, M.I. Danila, K.G. Saag, M. Rossini, Osteoporosis in 10 years time: a glimpse into the future of osteoporosis, Ther. Adv. Musculoskelet. Dis. 14 (2022) 1759720×221083541.

[21] A.W. James, G. LaChaud, J. Shen, G. Asatrian, V. Nguyen, X. Zhang, K. Ting, C. Soo, A review of the clinical side effects of bone morphogenetic protein-2, Tissue Eng. Part B Rev. 22 (4) (2016) 284–297.

[22] N. Percie du Sert, A. Ahluwalia, S. Alam, M.T. Avey, M. Baker, W.J. Browne, A. Clark, I.C. Cuthill, U. Dirnagl, M. Emerson, P. Garner, S.T. Holgate, D.W. Howells, V. Hurst, N.A. Karp, S.E. Lazic, K. Lidster, C.J. MacCallum, M. Macleod, E.J. Pearl, O.H. Petersen, F. Rawle, P. Reynolds, K. Rooney, E.S. Sena, S.D. Silberberg, T. Steckler, H. Würbel, Reporting animal research: explanation and elaboration for the ARRIVE guidelines 2.0, PLoS Biol. 18 (7) (2020) e3000411.

[23] M.F. Pittenger, A.M. Mackay, S.C. Beck, R.K. Jaiswal, R. Douglas, J.D. Mosca, M.A. Moorman, D.W. Simonetti, S. Craig, D.R. Marshak, Multilineage potential of adult human mesenchymal stem cells, Science 284 (5411) (1999) 143–147.

[24] M.A. Miller, A. Ivkovic, R. Porter, M.B. Harris, D.M. Estok 2nd, R.M. Smith, C.H. Evans, M.S. Vrahas, Autologous bone grafting on steroids: preliminary clinical results. A novel treatment for nonunions and segmental bone defects, Int. Orthop. 35 (4) (2011) 599–605.

[25] H. Schepler, M. Neufurth, S. Wang, Z. She, H.C. Schröder, X. Wang, W.E.G. Müller, Acceleration of chronic wound healing by bio-inorganic polyphosphate: in vitro studies and first clinical applications, Theranostics 12 (1) (2022) 18–34.

[26] W.E.G. Müller, M. Ackermann, B. Al-Nawas, L.A.R. Righesso, R. Muñoz-Espí, E. Tolba, M. Neufurth, H.C. Schröder, X. Wang, Amplified morphogenetic and bone forming activity of amorphous versus crystalline calcium phosphate/polyphosphate, Acta Biomater. 118 (2020) 233–247.

[27] W.E.G. Müller, E. Tolba, H.C. Schröder, R. Muñoz-Espí, B. Diehl-Seifert, X. Wang, Amorphous polyphosphate-hydroxyapatite: a morphogenetically active substrate for bone-related SaOS-2 cells in vitro, Acta Biomater. 31 (2016) 358–367.

[28] J. Visser, D. Gawlitta, K.E. Benders, S.M. Toma, B. Pouran, P.R. van Weeren, W.J. Dhert, J. Malda, Endochondral bone formation in gelatin methacrylamide hydrogel with embedded cartilage-derived matrix particles, Biomaterials 37 (2015) 174–182.

[29] S.L. Cheng, J.W. Yang, L. Rifas, S.F. Zhang, L.V. Avioli, Differentiation of human bone marrow osteogenic stromal cells in vitro: induction of the osteoblast phenotype by dexamethasone, Endocrinology 134 (1) (1994) 277–286.

[30] D.P. Hu, F. Ferro, F. Yang, A.J. Taylor, W. Chang, T. Miclau, R.S. Marcucio, C.S. Bahney, Cartilage to bone transformation during fracture healing is coordinated by the invading vasculature and induction of the core pluripotency genes, Development 144 (2) (2017) 221–234.

[31] S.A. Wong, K.O. Rivera, T. Miclau, E. Alsberg, R.S. Marcucio, C.S. Bahney, Microenvironmental regulation of chondrocyte plasticity in endochondral repair—a new frontier for developmental engineering, Front. Bioeng. Biotechnol. 6 (2018).

[32] H.J. Yan, T. Casalini, G. Hulsart-Billström, S. Wang, O.P. Oommen, M. Salvalaglio, S. Larsson, J. Hilborn, O.P. Varghese, Synthetic design of growth factor sequestering extracellular matrix mimetic hydrogel for promoting in vivo bone formation, Biomaterials 161 (2018) 190–202.

[33] M. Yamamoto, Y. Tabata, Y. Ikada, Ectopic bone formation induced by biodegradable hydrogels incorporating bone morphogenetic protein, J. Biomater. Sci. Polym. Ed. 9 (5) (1998) 439–458.

[34] D. Lantigua, X. Wu, S. Suvarnapathaki, M.A. Nguyen, G. Camci-Unal, Composite scaffolds from gelatin and bone meal powder for tissue engineering, Bioengineering 8 (11) (2021).

[35] M.A. Podestà, G. Remuzzi, F. Casiraghi, Mesenchymal stromal cells for transplant tolerance, Front. Immunol. 10 (2019) 1287.

[36] T. Thitiset, S. Damrongsakkul, S. Yodmuang, W. Leeanansaksiri, J. Apinun, S. Honsawek, A novel gelatin/chitooligosaccharide/demineralized bone matrix composite scaffold and periosteum-derived mesenchymal stem cells for bone tissue engineering, Biomater. Res. 25 (1) (2021) 19.

[37] K. Schmidt-Bleek, B.J. Kwee, D.J. Mooney, G.N. Duda, Boon and bane of inflammation in bone tissue regeneration and its link with angiogenesis, Tissue Eng. Part B Rev. 21 (4) (2015) 354–364.

[38] C. Schlundt, S. Reinke, S. Geissler, C.H. Bucher, C. Giannini, S. Märdian, M. Dahne, C. Kleber, B. Samans, U. Baron, G.N. Duda, H.D. Volk, K. Schmidt-Bleek, Individual effector/regulator t cell ratios impact bone regeneration, Front. Immunol. 10 (2019) 1954.

[39] S. Fujiwara, Humanized mice: a brief overview on their diverse applications in biomedical research, J. Cell. Physiol. 233 (4) (2018) 2889–2901.

[40] D.S. Garske, K. Schmidt-Bleek, A. Ellinghaus, A. Dienelt, L. Gu, D.J. Mooney, G.N. Duda, A. Cipitria, Alginate hydrogels for in vivo bone regeneration: the immune competence of the animal model matters, Tissue Eng. Part A 26 (15-16) (2020) 852–862.

[41] M.J. McClure, L.C. Olson, D.J. Cohen, Y.C. Huang, S. Zhang, T. Nguyen, B.D. Boyan, Z. Schwartz, RNU (Foxn1 (RNU)-Nude) rats demonstrate an improved ability to regenerate muscle in a volumetric muscle injury compared to sprague dawley rats, Bioengineering 8 (1) (2021).

[42] B.S. Kim, F. Shkembi, J. Lee, In vitro and in vivo evaluation of commercially available fibrin gel as a carrier of alendronate for bone tissue engineering, Biomed. Res. Int. 2017 (2017) 6434169.

[43] K. Komatsu, T. Shibata, A. Shimada, H. Ideno, K. Nakashima, Y. Tabata, A. Nifuji, Cationized gelatin hydrogels mixed with plasmid DNA induce stronger and more sustained gene expression than atelocollagen at calvarial bone defects in vivo, J. Biomater. Sci. Polym. Ed. 27 (5) (2016) 419–430.

[44] S. Lin, L. Cao, Q. Wang, J. Du, D. Jiao, S. Duan, J. Wu, Q. Gan, X. Jiang, Tailored biomimetic hydrogel based on a photopolymerised DMP1/MCF/gelatin hybrid system for calvarial bone regeneration, J. Mater. Chem. B 6 (3) (2018) 414–427.

[45] M.C. Chen, H.C. Chiu, P.J. Kuo, C.Y. Chiang, M.M. Fu, E. Fu, Bone formation with functionalized 3D printed poly-ε-caprolactone scaffold with plasma-rich-fibrin implanted in critical-sized calvaria defect of rat, J. Dent. Sci. 16 (4) (2021) 1214–1221.

[46] Y. Zhang, H. Leng, Z. Du, Y. Huang, X. Liu, Z. Zhao, X. Zhang, Q. Cai, X. Yang, Efficient regeneration of rat calvarial defect with gelatin-hydroxyapatite composite cryogel, Biomed. Mater. 15 (6) (2020) 065005.
[47] J. Yeom, B.W. Hwang, D.J. Yang, H.I. Shin, S.K. Hahn, Effect of osteoconductive hyaluronate hydrogels on calvarial bone regeneration, Biomater. Res. 18 (2014) 8.
[48] O.B. Agrali, S. Yildirim, H.O. Ozener, K.N. Köse, D. Ozbeyli, M. Soluk-Tekkesin, L. Kuru, Evaluation of the effectiveness of esterified hyaluronic acid fibers on bone regeneration in rat calvarial defects, Biomed. Res. Int. 2018 (2018) 3874131.
[49] Z. Li, J.A. Helms, Drill hole models to investigate bone repair, Methods Mol. Biol. 2221 (2021) 193–204.